Synthesis of Crystallized Mesoporous Tantalum Oxide and Its Photocatalytic Activity for Overall Water Splitting under Ultraviolet Light Irradiation

Yu Noda,[†,§] Byongjin Lee,[†] Kazunari Domen,[†] and Junko N. Kondo*[,‡]

Department of Chemical System Engineering, School of Engineering, The University of Tokyo, 7-3-1 Hongo, Bunkyo-ku, Tokyo 113-8656, Japan, and Chemical Resources Laboratory, Tokyo Institute of Technology, 4259 Nagatsuta, Midori-ku, Yokohama 226-8503, Japan

Received November 9, 2007. Revised Manuscript Received June 4, 2008

The well-ordered two-dimensional hexagonal (2D-hex) structure of mesoporous Ta_2O_5 was maintained after crystallization with the aid of SiO_2 reinforcement, which was removed after crystallization. The photocatalytic activity of the mesoporous Ta_2O_5 for overall water splitting under ultraviolet (UV) irradiation was improved by changing the solid phase structure from amorphous to crystalline by nearly 1 order of magnitude. The resulting photocatalytic activity of NiO_x(3.0 wt %)-loaded crystalline mesoporous Ta_2O_5 for water decomposition (3360 μmol·h^{-1} of H_2 and 1630 μmol·h^{-1} of O_2 evolution at the initial 1 h) was found to show one of the highest activities among so far reported photocatalysts under similar conditions. The high activity is attributable to the efficient transfer of the excited electrons and holes from inside to the surface of the catalyst through thin-walled crystalline phase.

1. Introduction

The unique characteristics of mesoporous materials are expected to contribute to potential applications such as catalysts, molecular sieves, sensors, and other nano devices.[1–3] While many researches have focused on silica-based materials,[4–7] many efforts have also been made to synthesize nonsilica materials[8–12] including transition-metal oxides,[11,12] which frequently have superior properties for catalysis. As an application of mesoporous metal oxides, we have reported that mesoporous Ta_2O_5 and Mg−Ta mixed oxide are efficient photocatalysts for water splitting under UV irradiation.[13–15] The selection of the photocatalytic water splitting is based on the consideration that it might promise stable hydrogen production by sunlight energy conversion. Although the walls of these oxides were amorphous, both of them exhibited higher activity than the crystallized nonporous Ta_2O_5 and $MgTa_2O_6$, respectively. The advantage of mesoporous structure originates from their very thin walls, where only a short distance lies for the photoexcited electrons and holes to reach the surface compared to nonporous samples. The resultant short resident time of electrons and holes in bulk reduces the possibility for recombination and enables the more efficient photocatalytic reaction. Other researchers also have studied the advantageous characteristics of mesoporous Ta and Ta-based oxides, targeting other reactions such as the conversion of dinitrogen to ammonia.[16–19]

The amorphous state of most of the as-made mesoporous oxides limits their catalytic performances due to relatively poor thermal and mechanical stabilities as well as insufficient electric and optical performance. Crystalline solids, on the other hand, have much better stabilities and frequently superior catalytic properties, which are derived from specific electronic orbitals and/or lattice defects. It is generally known that high crystallinity in solids leads to high photocatalytic activity because photoexcited electrons and holes can be transferred to the surface with higher velocity, which decreases the recombination opportunity. For example, anatase TiO_2 showed higher photocatalytic activity for

* To whom correspondence should be addressed. Fax: +81-45-924-5282. Tel.: 81-45-924-5239. E-mail: jnomura@res.titech.ac.jp.
† The University of Tokyo.
‡ Tokyo Institute of Technology.
§ Present address: Department of Energy and Mineral Engineering, The Pennsylvania State University, University Park, PA 16802.

(1) Davis, M. E. *Nature* **2002**, *417*, 813.
(2) Yamada, T.; Zhou, H. S.; Uchida, H.; Tomita, M.; Ueno, Y.; Ichino, T.; Honma, I.; Asai, K.; Katsube, T. *Adv. Mater.* **2002**, *14*, 812.
(3) Kavan, L.; Rathousky, J.; Grätzel, M.; Shklover, V.; Zukal, A. *Microporous Mesoporous Mater.* **2001**, *44*, 653.
(4) Kresge, C. T.; Leonowicz, M. E.; Roth, W. J.; Vartuli, J. C.; Beck, J. S. *Nature* **1992**, *359*, 710.
(5) Attard, G. S.; Glyde, J. C.; Goltner, C. G. *Nature* **1995**, *378*, 366.
(6) Templin, M.; Franck, A.; Chesne, A. D.; Leist, H.; Zhang, Y.; Ulrich, R.; Schädler, V.; Wiesner, U. *Science* **1997**, *278*, 1795.
(7) Zhao, D.; Feng, J.; Huo, Q.; Melosh, N.; Fredrickson, G. H.; Chmelka, B. F.; Stucky, G. D. *Science* **1998**, *279*, 548.
(8) Ying, J. Y.; Mehnert, C. P.; Wong, M. S. *Angew. Chem., Int. Ed.* **1999**, *38*, 56.
(9) Yu, C.; Tian, B.; Zhao, D. *Curr. Opin. Solid State Mater. Sci.* **2003**, *7*, 191.
(10) Palmqvist, A. E. C. *Curr. Opin. Colloid Interface Sci.* **2003**, *8*, 145.
(11) Yang, P.; Zhao, D.; Margolese, D. I.; Chmelka, B. F.; Stucky, G. D. *Nature* **1998**, 396.
(12) Yang, P.; Zhao, D.; Margolese, D. I.; Chmelka, B. F.; Stucky, G. D. *Chem. Mater.* **1999**, *11*, 2813.
(13) Takahara, Y.; Kondo, J. N.; Takata, T.; Lu, D.; Domen, K. *Chem. Mater.* **2001**, *13*, 1194.
(14) Uchida, M.; Kondo, J. N.; Lu, D.; Domen, K. *Chem. Lett.* **2002**, 498.
(15) Kondo, J. N.; Uchida, M.; Nakajima, K.; Lu, D.; Hara, M.; Domen, K. *Chem. Mater.* **2004**, *16*, 4304.
(16) Lezau, A.; Skadtchenko, B.; Trudeau, M.; Antonelli, D. M. *J. Chem. Soc., Dalton Trans.* **2003**, 4115.
(17) Yue, C.; Trudeau, M. L.; Antonelli, D. *Can. J. Chem.* **2005**, *83*, 308.
(18) Yue, C.; Trudeau, M.; Antonelli, D. *Chem. Commun.* **2006**, 1918.
(19) Yue, C.; Qiu, L.; Trudeau, M.; Antonelli, D. *Inorg. Chem.* **2007**, *46*, 5084.

10.1021/cm703202n CCC: $40.75
Published on Web 07/29/2008

oxidative dehydrogenation of 2-propanol than mesoporous TiO_2 with an amorphous wall structure.[20] Accordingly, crystallization of as-made mesoporous materials is of great importance, including the case of mesoporous Ta_2O_5. It should be noted that mesoporous Ta_2O_5, being different from TiO_2, shows high activity regardless of its amorphous structure. We have supposed that the high photocatalytic performance of amorphous mesoporous Ta_2O_5 can be attributable to its band structure.[13] The relatively higher LUMO level of Ta_2O_5 than that of TiO_2 is able to generate excited electrons in a higher potential and overcome the activation energy of the reaction. Thus, the electronic characteristics as well as the mesoporous structure is significant for the high activity of mesoporous Ta_2O_5. Therefore, if mesoporous oxides are successfully crystallized, keeping the mesoporosity, we can expect much better catalytic performances especially from Ta-based oxides. While the utilization of visible light for water decomposition has been extensively studied using (oxy)nitrides,[21,22] (oxy)sulfides,[23,24] and as a modified $TiSi_2$ catalyst,[25] the application of mesoporous materials to photochemistry is attempted in the present study from the viewpoint of inorganic atomic structure (crystallinity).

Calcination at high temperatures, which is required for crystallization, causes vigorous mass transfer to collapse the mesoporous structure with a significant loss in surface area. Fortifying the pore walls before crystallization is regarded as an effective approach. In our previous study, carbon was applied to be filled into the pores of 2D-hex mesoporous Nb−Ta mixed oxide. Then, the carbon-filled sample was crystallized by calcination in an inert atmosphere followed by removal of carbon by calcination in air.[26] The carbon-filling method prior to crystallization proved to be effective for preservation of the original mesoporous structure to some extent. Still, it was difficult to fill the pores with carbon completely, and the method could not be applied for all the mesoporous metal oxides. Recently, we established a new crystallization method using a silicone compound to form SiO_2 layers that strengthen the surface of pore walls.[27] In the study, 1,1,1,3,5,5,5-heptamethyltrisiloxane ($[(CH_3)_3SiO]_2SiHCH_3$) was used to treat an as-made mesoporous sample in advance of calcination. The Si−H bond of siloxane reacted with the hydroxyl groups on the surface of the oxide (M−OH, M = metal cation) and then Si atoms were chemically combined with the pore walls by M−O−Si bonds. Furthermore, it was revealed that adsorbed siloxane molecules and the derivatives of the self-reacted siloxane remained on the surface and these additional SiO_2 sources were significant in forming thick layers to fortify the structure stably. The successive calcination caused combustion of the methyl groups and formation of SiO_2. These SiO_2 layers restricted the mass transfer during crystallization and thus successfully prevented pore collapse. Previous works concentrated on the materials preparation, and no catalytic performances of these crystallized mesoporous materials were examined. In the present work, crystallized mesoporous Ta_2O_5 was synthesized following SiO_2-reinforcement method and its photocatalytic activity for overall water splitting under UV irradiation was evaluated. Thus, the purpose of the present study is to evaluate the improvement of photocatalytic activity upon crystallization, which is directly related to the velocity of electrons and holes in amorphous and crystalline bulk structures, rather than to utilize the visible light. Since photocatalytic water splitting is frequently promoted by loading an appropriate cocatalyst, the activities of the samples loaded with some different cocatalyts (NiO, NiO_x, RuO_2, and $Rh_{2-y}Cr_yO_3$) were also investigated.

2. Experimental Section

2.1. Chemicals. Tantalum pentachloride, $TaCl_5$ (99.99%), was purchased from Kojundo Chemical Laboratory Co., Ltd. A structure-directing agent, poly block copolymer surfactant ($(HO(CH_2CH_2O)_{20}(CH_2CH(CH_3)O)_{70}(CH_2CH_2O)_{20}H$, Pluronic P-123), 1,1,1,3,5,5,5-heptamethyltrisiloxane ($[(CH_3)_3SiO]_2SiHCH_3$, 97%), and $Ru_3(CO)_{12}$ were obtained from Aldrich. $Ni(NO_3)_3\cdot 6H_2O$ (99.9%) and $Cr(NO_3)_3\cdot 9H_2O$ (99.9%) were obtained from Wako Pure Chemical Industries, Ltd. Dehydrated EtOH (99.5%), $Na_3RhCl_6\cdot 2H_2O$ (97%), and NaOH (97%) were purchased from Kanto Chemical Co., Inc. All chemicals were used as-received without further purification.

2.2. Synthesis. As an amorphous precursor, 2D-hex mesoporous Ta_2O_5 was synthesized by the previously reported method.[28] As a silicone treatment,[29] the amorphous precursor (1 g) was added to 1,1,1,3,5,5,5-heptamethyltrisiloxane (3 g) and stirred at 343 K for 12 h. The solid precipitate was then dried at 473 K for 1 h under evacuation to remove unreacted silicone constituent and crystallized by calcination in air at 1133 K for 1 h. For removal of the SiO_2 layers, the sample was treated with 1.5 M NaOH solution (pH 14) at 343 K for 60 min several times, until no Si was detected in the NaOH solution after the treatment. It is mentioned that Ta was absent in post-treated NaOH solution, indicating that Ta_2O_5 was not dissolved under the present condition. The NaOH-treated sample was then rinsed with pure water, and the final product was obtained after filtration and drying procedures. Although the presence/absence of Si in mesoporous Ta_2O_5 in the final product was not confirmed by elemental analyses (energy-dispersive X-ray spectroscopy, EDS) using a TEM apparatus because of the overlapping of characteristic peaks of Si and Ta, the averaged silicon content of other crystalline mesoporous transition metal oxides was less than 2% of the total metal element content. Thus, SiO_2 reinforcement is regarded as negligible on the final crystalline mesoporous Ta_2O_5 prepared in the present study.

2.3. Characterization. Powder X-ray diffraction (XRD) measurements were performed using a Rigaku RINT-UltimaIII Bragg-Brentano type X-ray diffractometer (Cu Kα radiation, 40 kV, 40 mA) at 0.01 step size and a 1 s step time over the range $0.3° < 2\theta < 7°$ and at the scanning rate of 4.0° min^{-1} over the range $10° < 2\theta < 60°$. N_2 adsorption−desorption isotherms at 77 K were

(20) Stone, V. F., Jr.; Davis, R. J. *Chem. Mater.* **1998**, *10*, 1468.
(21) Maeda, K.; Teramura, K.; Lu, D.; Takata, T.; Saito, N.; Inoue, Y.; Domen, K. *Nature* **2006**, *440*, 295.
(22) Maeda, K.; Hashiguchi, H.; Masuda, H.; Abe, R.; Domen, K. *J. Phys. Chem. C* **2008**, *112*, 3447.
(23) Kudo, A. *Int. J. Hydrogen Energy* **2007**, *32*, 2673.
(24) Kudo, A. *Pure Appl. Chem.* **2007**, *79*, 1917.
(25) Ritterskamp, P.; Kuklya, A.; Wüstkamp, M.; Kerpen, K.; Weidenthaler, C.; Demuth, M. *Angew. Chem., Int. Ed.* **2007**, *46*, 7770.
(26) Katou, T.; Lee, B.; Lu, D.; Kondo, J. N.; Hara, M.; Domen, K. *Angew. Chem., Int. Ed.* **2003**, *42*, 2382.
(27) Shirokura, N.; Nakajima, K.; Nakabayashi, A.; Lu, D.; Hara, M.; Domen, K.; Tatsumi, T.; Kondo, J. N. *Chem. Commun.* **2006**, 2188.
(28) Nakajima, K.; Hara, M.; Domen, K.; Kondo, J. N. *Chem. Lett.* **2005**, *34*, 394.
(29) Takata, T.; Furumi, Y.; Shinohara, K.; Tanaka, A.; Hara, M.; Kondo, J. N.; Domen, K. *Chem. Mater.* **1997**, *9*, 1063.

measured using BEL Japan BELSORP-mini after the pretreatment of 30 min degassing at 423 K under evacuation. The Brunauer, Emmett, Teller (BET) surface areas were estimated over the range of relative pressure (P/P_0) from 0.1 to 0.5. Transmission electron microscopy (TEM) observations were carried out using JEOL JEM-2010F. Crystallization temperature of amorphous mesoporous Ta_2O_5 was measured on a Shimadzu DTG-50/50H. X-ray photoelectron spectroscopy (XPS) measurements were performed on a JEOL JPS-90SX to investigate the state of NiO_x cocatalyst before and after the photocatalytic reaction.

2.4. Photocatalytic Reactions. Photocatalytic water splitting reactions were performed in a quartz inner irradiation-type reaction vessel connected to a closed gas circulation system (pressure <101.325 kPa).[13] The system was evacuated several times to remove residual air in a solution prior to light irradiation. Each reaction was carried out using 0.3 g of the photocatalyst suspended by magnetic stirring (F-205, Tokyo Garasu Kikai, stirring rate 1500 rpm) in 400 mL of pure water after evacuation of the system and irradiation under a 450 W high-pressure Hg lamp (λ > 200 nm). The evolved gases were analyzed using a gas chromatograph (MS-5A column, Ar gas as the carrier) through a gas sampler (10 cm^3 in volume) which was directly connected to the reaction system to avoid contamination from air.

Each NiO-, NiO_x-, and $Rh_{2-y}Cr_yO_3$-cocatalyst was loaded by an impregnation method. $Ni(NO_3)_3 \cdot 6H_2O$, $Cr(NO_3)_3 \cdot 9H_2O$, and $Na_3RhCl_6 \cdot 2H_2O$ were used as precursors to prepare aqueous solutions. Photocatalyst powder was immersed in each solution and dried followed by calcination in air. NiO was prepared by calcination at 573 K for 1 h, and to prepare NiO_x, subsequent H_2 (20 kPa) reduction at 673 K for 2 h and reoxidation in O_2 (10 kPa) at 473 K for 1 h were carried out. In this article, this reduction−reoxidation treatment for preparation of NiO_x cocatalyst is abbreviated as R673−O473 treatment. $Rh_{2-y}Cr_yO_3$ was obtained by calcination at 623 K for 1 h. In case of RuO_2, a metal precursor, $Ru_3(CO)_{12}$, was dissolved in tetrahydrofuran (THF). Photocatalyst powder was immersed in the solution and stirred at 333 K for 5 h. To remove THF, the solution was then dried and heated in air at 373 K for 1 h. The powder was subsequently calcined in air at 623 K for 1 h to form RuO_2.

3. Results and Discussion

3.1. Physical Properties of Mesoporous Ta_2O_5. Figure 1 shows small- and wide-angle XRD patterns of various mesoporous Ta_2O_5 at the steps of the crystallization procedure. For the as-synthesized precursor (Figure 1a), a diffraction peak was observed at θ = 1.3° due to the mesostructure, and the absence of any peaks at wide angles indicates the amorphous feature. Crystallization after the silicone treatment and SiO_2 removal gave no significant change in XRD patterns at small angles (Figures 1b and 1c), supporting the preservation of the original mesoporous framework, although the peaks were slightly shifted to 1.4° after crystallization. Diffraction peaks in the wide-angle region are attributed to crystalline Ta_2O_5 (orthorhombic). Thus, the calcination of the samples at 1133 K for 1 h is confirmed to be a sufficient condition for crystallization of mesoporous Ta_2O_5. On the other hand, for the sample crystallized without any treatment (Figure 1d), no peak at small angles was observed, indicating the collapse of the mesoporous framework. Therefore, strengthening the pore structure by the silicone treatment is demonstrated to be effective for the preservation of mesoporosity during crystallization.

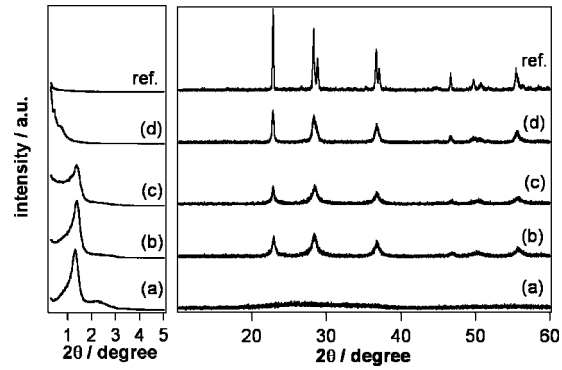

Figure 1. Small- and wide-angle XRD patterns of (a) the amorphous precursor, (b) the crystallized sample after silicone treatment, (c) the alkaline-treated crystallized sample, and (d) the crystallized sample without silicone treatment. The reference Ta_2O_5 was purchased from High Purity Chemicals.

Table 1. Physical Properties of Amorphous and Crystallized Mesoporous Ta_2O_5

sample	S_{BET}/ $m^2 \cdot g^{-1}$	pore size/ nm	pore volume/ $mL \cdot g^{-1}$	repeat distance/nm
amorphous precursor	131	4.8	0.18	6.7
silicone-treated sample	74	3.3	0.08	7.0
crystallized sample after silicone treatment	81	3.3	0.09	6.4
alkaline-treated crystallized sample	109	3.7	0.14	6.4
crystallized sample without silicone treatment	6		0.05	

N_2 adsorption−desorption isotherms of each sample in the crystallization procedure are shown in Figure 2, and physical properties obtained from XRD and N_2 sorption measurements are summarized in Table 1. The isotherm for the amorphous precursor (Figure 2a) is analogous to the type-IV isotherm pattern peculiar to mesoporous materials. The pore size is estimated as 4.8 nm from N_2 uptake at P/P_0 = 0.5−0.6. As shown in Figure 2d, direct crystallization without the silicone treatment caused pore collapse, which is found from the flat N_2 adsorption uptake at P/P_0 < 0.8. This is consistent with

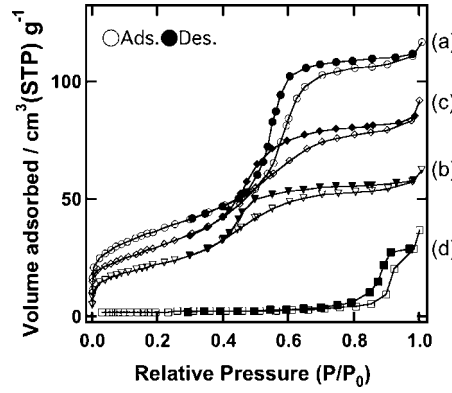

Figure 2. N_2 adsorption−desorption isotherms of (a) the amorphous precursor, (b) the crystallized sample after silicone treatment, (c) the alkaline-treated crystallized sample, and (d) the crystallized sample without silicone treatment.

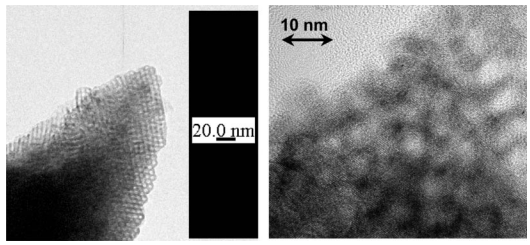

Figure 3. TEM images of crystallized mesoporous Ta_2O_5 after the alkali treatment.

the XRD pattern (Figure 1d), and the surface area significantly decreased from 131 to 6 $m^2 \cdot g^{-1}$. Meanwhile, the samples crystallized after the silicone treatment and further SiO_2 removal exhibited type-IV isotherm patterns (Figures 2b and 2c). In a comparison of the physicochemical properties in Table 1, surface area at first decreased to 74 $m^2 \cdot g^{-1}$ by the silicone treatment, slightly increased after crystallization to 81 $m^2 \cdot g^{-1}$, and recovered up to 109 $m^2 \cdot g^{-1}$ after the removal of SiO_2 layers. The pore volume was clearly reflected by the presence/absence of the reinforcement; it decreased after silicone treatment and recovered after SiO_2 removal. Repeat distance did not change much throughout all the procedures.

TEM images of the sample after SiO_2 removal are shown in Figure 3. 2D-hex ordered mesopores are clearly observed on the left image, while lattice fringes due to a crystalline structure are recognized on the right image together with some mesopores. From these images copresence of the ordered mesoporous structure at nanometer size order and crystalline structure at subnanometer order is evidenced. Thus, SiO_2-reinforcement method is effective at maintaining the original mesoporous structure throughout the crystallization process. The crystallized mesoporous Ta_2O_5 is successfully synthesized by this SiO_2 reinforcement method.

3.2. High Activity of NiO_x-Loaded Crystallized Mesoporous Ta_2O_5. It is known that NiO is the most effective cocatalyst for $K_2La_2Ti_3O_{10}$,[29] $K_4Nb_6O_{17}$, and pure Ta_2O_5,[30] and that reduction and reoxidation (R673−O473) treatment of NiO cocatalyst to form NiO_x improves the activity. The pretreatment produces Ni metal particles covered with NiO on the main photocatalysts; the first reduction by H_2 produces Ni metal particles and the successive oxidation by O_2 under a milder condition oxidizes only the surface of the Ni metal particle. The Ni metal part makes an ohmic contact between oxide photocatalyst and NiO. Thus, the excited electrons are smoothly transferred to the NiO surface to reduce water into H_2. This unique structure of NiO/Ni particles results in the enhancement of the photocatalytic activity. A typical time course of water splitting over NiO_x-loaded crystallized mesoporous Ta_2O_5 is shown in Figure 4, where NiO_x cocatalyst was prepared by R673−O473 treatment after NiO loading. Over NiO_x-loaded crystallized mesoporous Ta_2O_5, H_2 and O_2 evolved stoichiometrically at rates of 3.4 and 1.6 $mmol \cdot h^{-1}$, respectively, in the first run for 1 h (Figure 4), but the rates of gas evolution significantly decreased with the time of the reaction. The deactivation is found to be attributed to the change in the state of NiO_x cocatalyst by the XPS study, which is discussed below. In Figure 5, the photocatalytic activities of three different NiO_x-loaded samples of mesoporous Ta_2O_5 are compared: (a) crystallized (orthorhombic) nonporous sample, (b) amorphous mesoporous sample, and (c) crystallized mesoporous sample. We previously reported amorphous mesoporous Ta_2O_5 prepared by the same method exhibited almost the same photocatalytic activity for overall water splitting as that over the crystallized nonporous sample in spite of its amorphous structure,[31] the reproducibility of

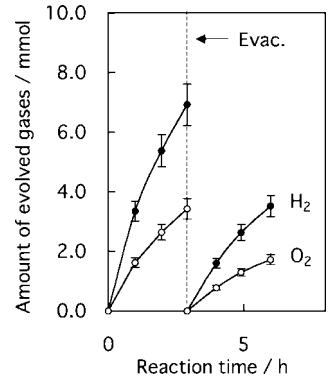

Figure 4. Time course of gas evolution from overall water splitting on crystallized mesoporous Ta_2O_5 loaded with NiO_x (3.0 wt % as NiO) under UV irradiation (λ > 200 nm).

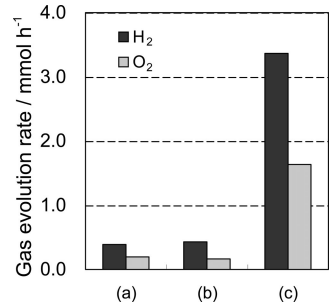

Figure 5. Photocatalytic activities of various Ta_2O_5 for overall water splitting under UV irradiation (λ > 200 nm). (a) Crystallized nonporous Ta_2O_5 loaded with NiO_x (1 wt % as NiO), (b) amorphous mesoporous Ta_2O_5 loaded with NiO_x (3 wt % as NiO), and (c) crystallized mesoporous Ta_2O_5 loaded with NiO_x (3 wt % as NiO).

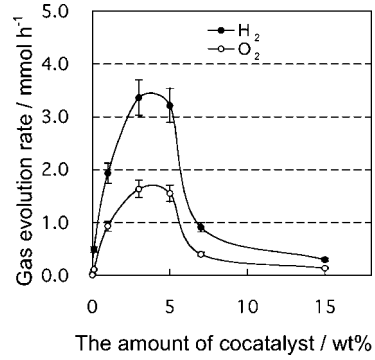

Figure 6. Dependence of the photocatalytic activity of crystallized mesoporous Ta_2O_5 for overall water splitting under UV irradiation (λ > 200 nm) on the loading amount of NiO_x. The amount of cocatalyst is estimated as NiO.

(30) Takata, T.; Tanaka, A.; Hara, M.; Kondo, J. N.; Domen, K. *Catal. Today* **1998**, *44*, 17.
(31) Nakajima, K.; Hara, M.; Domen, K.; Kondo, J. N. *Stud. Surf. Sci. Catal.* **2005**, *158*, 1477.
(32) Kato, H.; Kudo, A. *Chem. Phys. Lett.* **1998**, *295*, 487.

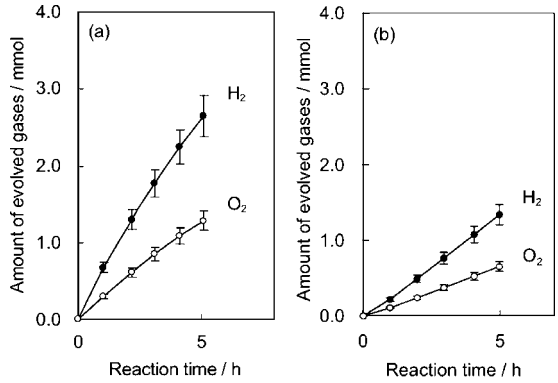

Figure 7. Time course of gas evolution from overall water splitting on crystallized mesoporous Ta_2O_5 loaded with (a) 3.0 wt % RuO_2 and (b) $Rh_{2-y}Cr_yO_3$ under UV irradiation ($\lambda > 200$ nm).

which is confirmed in Figure 5. Additionally, we revealed that the activity of the crystallized mesoporous sample synthesized by the SiO_2 reinforcement method is more than 7 times that of the amorphous mesoporous sample. Since the activity of the sample crystallized without the silicone treatment, which had no mesoporosity, was as low as that of the crystallized nonporous sample, it has been clarified that both crystallization and preservation of the mesoporous structure significantly contributed to the improvement of photocatalytic activity.

3.3. Effect of Cocatalyst Loading and R673−O473 Treatment. The dependence of the photocatalytic activity of crystallized mesoporous Ta_2O_5 on the amount of loading NiO_x cocatalyst (calculated as NiO) was studied (Figure 6). The activity significantly increased to a certain point with increasing the amount of loading, reaching the optimal amount at 3.0 wt %. The optimal amount is the same as the case of the amorphous mesoporous sample, while that of crystallized nonporous Ta_2O_5 is less than 1.0 wt %.[32]

The comparisons of photocatalytic activities of the amorphous and crystallized samples loaded with NiO_x together with the crystallized mesoporous Ta_2O_5 samples with various cocatalysts are summarized in Table 2. First, the crystallized sample without cocatalyst (run 4) showed extremely low activity and H_2 and O_2 did not evolve in stoichiometric ratio, which is the same tendency as the result of amorphous mesoporous Ta_2O_5 in the previous study.[31] In the case of the amorphous sample, NiO loading (without R673−O473 treatment) enabled the stoichiometric water splitting and notably improved the activity.[13] Nevertheless, NiO loading was not effective and the activity remained unchanged in the case of the crystallized sample as shown in Table 2 (runs 4 and 5). The activity was even lower than the reported one of the NiO-loaded amorphous sample.[31] Although the details of the mechanism are now under investigation, the silicone and following alkaline treatments may change the surface property of the catalyst to interfere with the migration of electrons and holes from the catalyst surface to the NiO cocatalyst. After R673−O473 treatment (run 6), on the other hand, the activity became higher than that before the treatment by 2 orders of magnitude. It is reported that R673−O473 treatment enhanced the activity of the NiO-loaded amorphous sample by no more than 4 times.[13,31] While the amorphous sample did not necessarily require

Table 2. Photocatalytic Activities of Amorphous and Crystallized Mesoporous Ta_2O_5

run[a]	cocatalyst	H_2 evolution rate/μmol·h^{-1}	O_2 evolution rate/μmol·h^{-1}
1	NiO_x[b]	390	190
2	NiO_x	430[c]	160[c]
3	NiO_x	760[c]	320[c]
4		30[c]	10[c]
5	NiO 3.0 wt %	30[c]	10[c]
6	NiO_x	3360[c]	1630[c]
7	3.0 wt % RuO_x	660[c]	290[c]
8	1.0 wt % Rh, 1.5 wt % Cr	270	130

[a] Run 1, nonporous Ta_2O_5 with NiO_x; run 2, amorphous precursor with NiO_x; run 3, silicone-treated crystallized sample with NiO_x; run 4, silica-free crystallized sample without cocatalyst; run 5, sample in run 4 with 3.0 wt % NiO; run 6, sample in run 5 after R673−O473 treatment; run 7, sample in run 4 with with 3.0 wt % RuO_2; run 8, sample in run 4 with 1.0 wt % Rh and 1.5 wt % Cr. [b] NiO_x cocatalyst is prepared by R672−O473 treatment of 3.0 wt % NiO-loaded sample. [c] The initial rates for 1 h.

R673−O473 treatment leading to the formation of NiO_x cocatalyst, it was indispensable for the high activity of the crystallized sample. Among various photocatalysts so-far reported, NiO(0.05 wt %)-loaded $NaTaO_3$ shows the highest activity for overall water splitting (2180 μmol·h^{-1} of H_2 and 1100 μmol·h^{-1} of O_2) under UV irradiation.[33] The activity of the presently prepared crystalline mesoporous Ta_2O_5 exceeds that of NiO(0.05 wt %)-loaded $NaTaO_3$, although a further modification increases the activity of NiO(0.05 wt %)-loaded $NaTaO_3$.[34] This demonstrates the advantage of the thin-walled mesoporous structure for photocatalysis.

Second, it should be noted that NiO_x-loaded crystallized sample before the alkaline treatment (run 3) also showed higher activity than the amorphous sample. The result seems inconsistent because the pore walls of the sample were still covered with SiO_2 layers, through which photoexcited electrons and holes are not able to migrate. We speculate that a part of Ta_2O_5 became exposed on the surface after calcination at high temperatures. Furthermore, O_2 evolution of most samples was relatively low compared to stoichiometric gas evolution. This tendency might be attributable to the possibility that photogenerated holes were used to oxidize residue of organic compounds on the catalyst surface.[13] Even in the cases of NiO_x-loaded samples, it is likely that the same process occurred but the effect was almost negligible due to the high activity. In general, excess H_2 evolution is sometimes observed for a water splitting reaction, the origin of which remains to be elucidated.[13,32,35–38] The same phenomenon was also observed for mesoporous Ta_2O_5,[13] which was attributed to the remaining surfactant-originated organic groups. In this case, the stoichiometry of H_2 and O_2 evolution was achieved in the time course, and this is also observed

(33) Kato, H.; Kudo, A. *Catal. Lett.* **1999**, *58*, 153.
(34) Kato, H.; Asakura, K.; Kudo, A. *J. Am. Chem. Soc.* **2003**, *125*, 3082.
(35) Maeda, K.; Saito, N.; Inoue, Y.; Domen, K. *Chem. Mater.* **2007**, *19*, 4092.
(36) Kato, H.; Kudo, A. *J. Phys. Chem. B* **2001**, *105*, 4285.
(37) Sato, J.; Kobayashi, H.; Saito, N.; Nishiyama, H.; Inoue, Y. *J. Photochem. Photobiol. A: Chem.* **2003**, *158*, 139.
(38) Sato, J.; Saito, N.; Nishiyama, H.; Inoue, Y. *J. Photochem. Photobiol. A: Chem.* **2002**, *148*, 85.

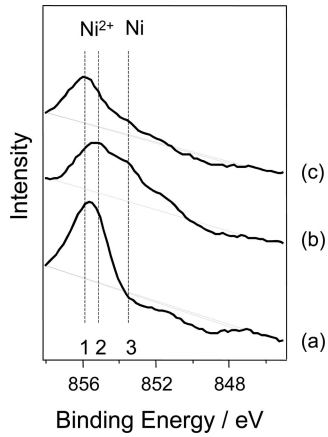

Figure 8. XPS spectra for Ni $2p_{3/2}$ of cocatalyst-loaded crystallized mesoposous Ta_2O_5 (a) before R673−O473 treatment, (b) after the treatment, and (c) after the 6 h photocatalytic reaction under UV irradiation.

in the present catalyst. The total organic carbon determination or the detection of CO_2 was not possible without detection/analysis setup.

Both of the RuO_2-loaded (run 7) and $Rh_{2-y}Cr_yO_3$-loaded (run 8) samples achieved water splitting under UV irradiation. While RuO_2 is known as a cocatalyst for Ta_2O_5[39] and other photocatalysts,[40–42] $Rh_{2-y}Cr_yO_3$ cocatalyst has been recently developed by our group particularly for a visible-light-driven photocatalyst $(Ga_{1-x}Zn_x)(N_{1-x}O_x)$,[43–45] which is also effective for some other photocatalysts.[45] We revealed in this study that $Rh_{2-y}Cr_yO_3$ is also applicable to mesoporous Ta_2O_5. The time courses of the reactions over the samples loaded with these two cocatalysts are shown in Figure 7. In either case, little or no deactivation was observed for the 5 h reaction, although the evolution rates for the first 1 h of the irradiation were both lower than that of the NiO_x-loaded sample as shown in Table 2. As the loading amount of these cocatalysts has not been optimized yet, much higher activity is still expected. These cocatalysts are still under examination.

3.4. XPS Measurements and TEM Observations of NiO_x Cocatalyst. XPS measurements and TEM observations were conducted to investigate the state of NiO_x cocatalyst dispersed onto the crystallized mesoporous Ta_2O_5. Figure 8 shows XPS spectra for Ni $2p_{3/2}$ of the sample (a) before R673−O473 treatment, (b) after the treatment, and (c) after the 6 h photocatalytic reaction under UV irradiation. For the sample before R673−O473 treatment, a clear peak was observed at 855.6 eV (peak 1). After the treatment, on the other hand, the peak slightly shifted to lower binding energy at 855.2 eV (peak 2), and another broad small peak appeared at 853.5 eV (peak 3). In the spectrum of the sample after the reaction, only one peak was observed at 855.7 eV. The reported value of binding energy for NiO is 854.5 eV, while

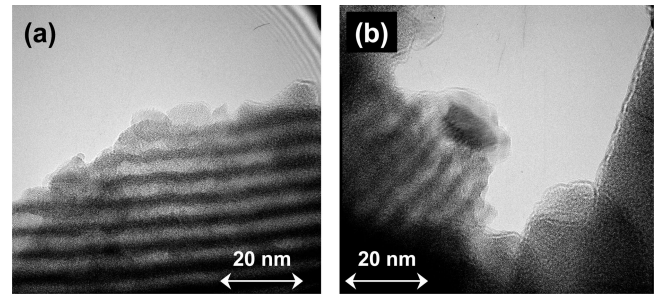

Figure 9. TEM images of (a) small and (b) large NiO_x particles loaded onto crystallized mesoporous Ta_2O_5.

that for NiO containing excess oxygen and Ni metal give peaks at 855.8 and 853.1 eV, respectively.[46] Considering these reported values, NiO cocatalyst before and after R673−O473 treatment is supposed to contain excess oxygen. The treatment then reduced NiO into Ni and partly oxidized Ni again to form the active NiO_x cocatalyst. Thus, the composite of metallic Ni and oxidized NiO was prepared as an active form, as shown above (section 3.2). It has been reported that the exterior surface of active NiO_x cocatalyst prepared by the same treatment on $SrTiO_3$ was covered with NiO and the interior of the NiO_x was dominated by Ni metal.[47] (The reduction and reoxidation temperatures in the case of $SrTiO_3$ were 773 and 473 K, respectively.) It is considered that this structure of NiO_x cocatalyst facilitates the transfer of electrons and holes from the catalyst surface to the cocatalyst and also prevents the reverse reaction of H_2 and O_2 to form H_2O. Thus, this structure of cocatalyst greatly enhances the photocatalytic activity. After the reaction, the peak assigned to Ni metal decreased in intensity and the Ni^{2+} state again became predominant. The disappearance of the peak of Ni metal may be attributed to the partial oxidation of Ni by the photoexcited holes or the growth of NiO layers that contain excess oxygen, resulting in masking of Ni metal atoms in the bulk. The reaction in water resulted in the loss of the peculiar structure of active NiO_x cocatalyst and the final state of the cocatalyst is found by XPS measurement to become similar to that before the treatment. Since there was no change observed in physical properties such as surface area and sorption isotherms of the samples before and after the reaction, this change in the Ni state is responsible for the degradation in the activity. The stability of RuO_2- and $Rh_{2-y}Cr_yO_3$-loaded samples supports this conclusion.

TEM images of the NiO_x-loaded samples are illustrated in Figure 9. Although many NiO_x small nanoparticles were dispersed onto the catalyst surface, some particles were found aggregated (Figure 9b). They were much larger than the size of the mesopores, which is approximately 4 nm. Small particles could have sintered during the reduction process of R673−O473 treatment. Sintering of Ni atoms during this process is reported in the previous XPS study[47] and supported by the present result, where the peak intensities for the sample after R673−O473 treatment and after the reaction were weakened compared to those before the treatment (Figure 8b and 8c). In general, aggregation of cocatalyst easily led to the decrease in the photocatalytic activity due to a fewer number of active sites, longer distance for electron

(39) Sayama, K.; Arakawa, H. *J. Photochem. Photobiol. A* **1994**, *77*, 243.
(40) Inoue, Y.; Kubokawa, T.; Sato, K. *J. Chem. Soc., Chem. Commun.* **1990**, 1298.
(41) Inoue, Y.; Asai, Y.; Sato, K. *J. Chem. Soc., Faraday Trans.* **1994**, *90*, 797.
(42) Sato, J.; Saito, N.; Nishiyama, H.; Inoue, Y. *J. Phys. Chem. B* **2001**, *105*, 6061.
(43) Maeda, K.; Teramura, K.; Takata, T.; Domen, K. *Nature* **2006**, 295.
(44) Maeda, K.; Teramura, K.; Lu, D.; Takata, T.; Saito, N.; Inoue, Y.; Domen, K. *J. Phys. Chem. B* **2006**, *110*, 13753.

charges to migrate, and hindrance for irradiation toward the catalyst. Obviously, nanoscale cocatalyst is more important especially for utilization of mesopore cavity. Thus, it is very likely that the conventional impregnation method and R673−O473 treatment are not the best for mesoporous catalysts. Thus, development of some other cocatalysts as well as novel loading methods would improve the dispersion of cocatalyst and the catalytic activity.

4. Conclusion

Successful crystallization of mesoporous Ta_2O_5 was achieved by reinforcement of amorphous mesoporous framework with SiO_2. The crystallized sample was shown to be an efficient photocatalyst for overall water splitting under UV light irradiation either with NiO_x, RuO_2, or $Rh_{2-y}Cr_yO_3$ cocatalyst. The photocatalytic activity of the NiO_x-loaded mesoporous Ta_2O_5 was improved to nearly 1 order of magnitude higher than that of the amorphous precursor by cystallization. To the best of our knowledge, this is the first report that describes the application of crystalline mesoporous transition metal oxide to photocatalysis due to the enhancement of photocatalytic characteristics by changing the solid phase structure of mesoporous materials.

CM703202N

(45) Maeda, K.; Teramura, K.; Saito, N.; Inoue, Y.; Domen, K. *J. Catal.* **2006**, *243*, 303.
(46) Wandelt, K. *Surf. Sci. Rep.* **1982**, *2*, 13, and references therein.
(47) Domen, K.; Kudo, A.; Onishi, T. *J. Phys. Chem.* **1986**, *90*, 292.